2013 IEEE/RSJ International Conference on
Intelligent Robots and Systems (IROS)
November 3-7, 2013. Tokyo, Japan

On Robot Dynamic Model Identification through Sub-Workspace Evolved Trajectories for Optimal Torque Estimation

Nicola Pedrocchi[1], Enrico Villagrossi[1,2], *Student Member, IEEE*, Federico Vicentini[1], *Member, IEEE* and Lorenzo Molinari Tosatti[1]

Abstract— **Model-based control are affected by the accuracy of dynamic calibration. For industrial robots, identification techniques predominantly involve rigid body models linearized on a set of minimal lumped parameters that are estimated along excitatory trajectories made by suitable/optimal path. Although the physical meaning of the estimated lumped models is often lost (*e.g.* negative inertia values), these methodologies get remarkably results when well-conditioned trajectories are applied. Nonetheless, such trajectories have usually to span the workspace at large, resulting in an averagely fitting model. In many technological tasks, instead, the region of dynamics applications is limited, and generation of trajectories in such workspace sub-region results in different specialized models that should increase the predictability of local behavior. Besides this consideration, the paper presents a genetic-based selection of trajectories in constrained sub-region. The methodology places under optimization paths generated by a commercial industrial robot interpolator, and the genes (*i.e.* the degrees-of-freedom) of the evolutionary algorithms corresponds to a finite set of few via-points and velocities, just like standard motion programming of industrial robots. Remarkably, experiments demonstrate that this algorithm design feature allows a good matching of foreseen current and the actual measured in different task conditions.**

I. Introduction

Trajectory optimization for excitatory patterns plays a dominant role in most of methods of dynamic calibration industrial robots (IRs). Since early examples [1], [2], [3], many calibration methods involve linear reduction of the rigid-body model into a set of dynamical parameters to be estimated in the sense of overdetermined systems from sampled torques along such excitatory trajectories. As a consequence, the accuracy of model estimations stands upon the conditioning properties of the kinematics function (regressor) that maps the to-be-estimated parameters into torques [4], [5]. Such implicit calibration procedure aims at attaining good *average* estimation properties in the whole workspace by building an extensively well-conditioned regressor, *i.e.* able to excite all linearly reduced dynamical parameters.

Within this general methodology, the optimization of excitatory trajectories has been addressed in many different approaches, *e.g.* optimization of trajectory parameters for polynomial [6] or Fourier series [7], [8]. The well-conditioning of such patterns have been often expressed through the conditioning number and the singular values [9], [10], [11], [12] of trajectory regressors to be optimally inverted. Some works [13], [14] soft-coded such properties in fitnesses functions for evolutionary-based techniques, which is also the case of the present work, but for oscillatory joint-space trajectories under optimization.

For such identification methods, the dynamical parameters observation produces the predicted torques with a configuration-dependent accuracy, *i.e.* the single average set of parameters is a tradeoff in the sense of least-squares or of optimal observers [11]. Drawbacks arise when the task patterns substantially differ from the original excitatory ones, since if the operation spans a limited sub-region of the workspace, it may happen that the corresponding regressor maps into the residuals of the estimated parameters. In other words, it could be inferred that the *local* validity of a calibration procedure in a sub-region of the workspace could benefit from a dedicated excitatory pattern. Such model is in general not valid at large and could even be potentially physically inconsistent with the system dynamics but well matching the numerical linear reduction of the dynamic parametrization. This useful loss of generality is of course suitable only in case of tasks performing very well defined classes of trajectories, as it may be the common case for a number of technological tasks, where the manipulator configuration is likely to change very little, *i.e.* the gravity term behaves as a nearly constant bias in the excitation.

The methodology proposed in this work aims at selecting a number of locally-optimal trajectories (task-oriented), for the estimation of robot dynamic parameters. The selection criteria is based on the evaluation of the excitation power on robot dynamic of each trajectory. Trajectories are defined likely in most manufacturing tasks, and, most importantly, encompass the standard task-space user-level programming of trajectories in most of commercial industrial controllers, *i.e.* a general trajectory is described by a set of discrete poses to be internally interpolated by the robot interpolator itself on the basis of global tunable parameters (fly-by accuracy, velocity profiles, etc). Since trajectories are obtained from an array of poses (and transit velocities), the template task description has a very limited complexity and is suitable for being embodied in an evolutionary optimization process where genomes directly code for such templates. As a result, the calibration problem is turned into a local *speciation* of the generalized excitatory acceleration able to provide the correspondingly speciated dynamical model. The evolutionary pressure will be, in fact, not on the real dynamical model

[1]N. Pedrocchi, *et al.* are with the Institute of Industrial Technologies and Automation, National Research Council, via Bassini 15, 20133 Milan, Italy
[2]E. Villagrossi is PhD Student with Università degli Studi di Brescia, Departement of Mechanical and Industrial Engineering, via Branze 39, 25123 Brescia, Italy
nicola.pedrocchi@itia.cnr.it

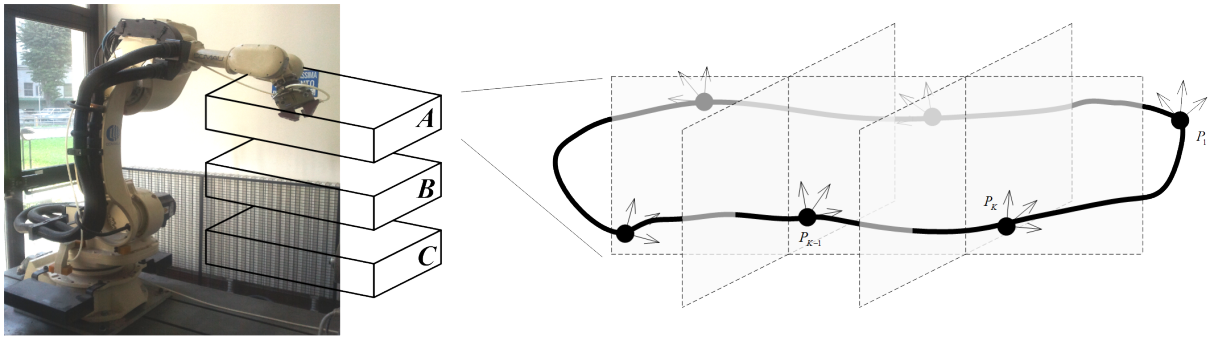

Fig. 1: Set of locations (left) where sub-regions of the workspace (***A***, ***B***, ***C***) are used to bound the spanning of K via-points, expressed as poses. Trajectories (right) are interpolated by the IRs controller along the via-points and according to motion laws coded into the genome in form of interpolation velocity.

but rather on the local set of best matching parameters in a given configuration. The *speciation* is seeked in 3 sub-regions of the same quadrant of the workspace (see Fig. 1). Such an experimental procedure aims at investigating the influence of the location where *speciation* takes place, in a fairly comparable robot conditions.

Section II will report the problem formulation in terms of linear system reduction, while the *speciation* methods will be outlined in Section II-B. Section III reports the results of the procedure applied to two differentn sub-regiorns of the task space. Section IV reports final considerations.

II. Motivation and Methodology

In most of dynamical parameters identifications, excitation trajectories are fairly different from those commonly used in industrial procedures, which are often characterized by classes of trajectories defined as sets of joined simple geometric entities (*e.g.* lines and circles), performed at constant regime velocity along the path. Alternatively, high accuracy in torques prediction could be obtained by Iterative Learning Control (ILC) techniques [15] resulting in implicit dynamics calibration, *i.e.* without the need of any model. Nevertheless, ILC algorithms prevent the possibility to extend (extrapolate) results for a given trajectory to similar ones, and are rarely used in tasks where robots have to interact with the environment [16]. Therefore, a sound algorithm for the local dynamics estimation requires both a proper dynamics model and a design method for excitatory trajectories that takes into account the constraints imposed by ranging within a small sub-region of the whole workspace in procedural mild-dynamics conditions. In addition, once designed and optimally computed, several trajectories representative of due tasks/sub-regions can be stored and loaded for re-calibration.

Notation

$\mathbf{q}_s = \left[q_s^1, .., q_s^{dof}\right]^t$	Joint positions at s-th sample time.
$\dot{\mathbf{q}}_s, \ddot{\mathbf{q}}_s, \boldsymbol{\tau}_s$	Velocities, accelerations, torques.
$\mathbf{Q} \equiv \{\mathbf{q}_1, .., \mathbf{q}_S\}$	Joint position time series of S different time samples.
$\{\mathbf{Q}, \dot{\mathbf{Q}}, \ddot{\mathbf{Q}}\}$	Trajectory.
$\tilde{(\cdot)}$, $\hat{(\cdot)}$, $(\cdot)^*$	Measured, estimated value and optimum estimation respectively.

A. Dynamics modeling and estimation

Making use of rigid multi-bodies dynamics [17], the robot dynamics can be reduced [18], [19] to:

$$\boldsymbol{\tau} = \boldsymbol{\phi}^0 \left(\ddot{\mathbf{q}}, \dot{\mathbf{q}}, \mathbf{q}\right) \boldsymbol{\pi}^0 \tag{1}$$

where $\boldsymbol{\pi}^0$ is a base set of dynamical parameters and matrix function $\boldsymbol{\phi}^0$ should be considered as generalized accelerations. The base set $\boldsymbol{\pi}^0$ includes only those parameters that give contribution to joint torques and are observable along any excitatory trajectory[1] that generates $\boldsymbol{\phi}^0$. The minimal size N_π of the base set $\boldsymbol{\pi}^0$ is demonstrated [11] to be 40 for a 6-dof anthropomorphic manipulator, in addition of which other N_f coefficients of the friction model yield the compound parameters set $\boldsymbol{\pi}$. The selected friction model [20] provides the j-th joint friction torque in the form:

$$\tau_f^j = f_0^j \, sign(\dot{q}^j) + f_1^j \dot{q}^j + f_2^j \, sign(\dot{q}^j) \left(\dot{q}^j\right)^2, \tag{2}$$

requiring $N_f = 3 \times dof$ additional parameters[2]. For trajectory $\{\mathbf{Q}, \dot{\mathbf{Q}}, \ddot{\mathbf{Q}}\}$ of S-samples, (1) is so expanded:

$$\mathbf{T} \equiv \begin{bmatrix} \boldsymbol{\tau}_1 \\ \vdots \\ \boldsymbol{\tau}_S \end{bmatrix} = \begin{bmatrix} \boldsymbol{\phi}_1 \left(\ddot{\mathbf{q}}_1, \dot{\mathbf{q}}_1, \mathbf{q}_1\right) \\ \vdots \\ \boldsymbol{\phi}_S \left(\ddot{\mathbf{q}}_S, \dot{\mathbf{q}}_S, \mathbf{q}_S\right) \end{bmatrix} \boldsymbol{\pi} = \boldsymbol{\Phi}\boldsymbol{\pi}, \tag{3}$$

where $\boldsymbol{\Phi}$ is the observation matrix. Actually, experimental sampling $\widetilde{\mathbf{T}}$, $\widetilde{\boldsymbol{\Phi}}$ includes also measurements noise $\boldsymbol{\nu}$:

$$\widetilde{\mathbf{T}} = \widetilde{\boldsymbol{\Phi}}\hat{\boldsymbol{\pi}} + \boldsymbol{\nu}, \quad \boldsymbol{\nu} \sim \mathcal{N}\left(0, \sigma_\nu\right). \tag{4}$$

Several techniques are known [21], [22], [23] for the pseudo-inversion solution of (4), and the weighted least-squares technique [24] has been here implemented. Denoting as $\boldsymbol{W}$ the weight matrix, the system is solved as

$$\hat{\boldsymbol{\pi}} = \left[(\widetilde{\boldsymbol{\Phi}}^t \boldsymbol{W} \widetilde{\boldsymbol{\Phi}})^{-1} \widetilde{\boldsymbol{\Phi}}^t \boldsymbol{W}\right] \widetilde{\mathbf{T}}. \tag{5}$$

Hence, the generation of an optimal excitation trajectory $\{\mathbf{Q}^\star, \dot{\mathbf{Q}}^\star, \ddot{\mathbf{Q}}^\star\}$ able to provide the best regression conditions for (4) leads the optimum parameters estimation.

[1]Dynamic calibration does not aim at estimating the full set of link figures (masses, inertias, friction coefficients) but to minimize the prediction error of the model w.r.t. the real behavior of the robot.

[2]For small movements friction has a remarkable relevance, overwhelming the contribution by other parameters and a standard linear friction, including the static and the viscous terms, appears to be inaccurate.

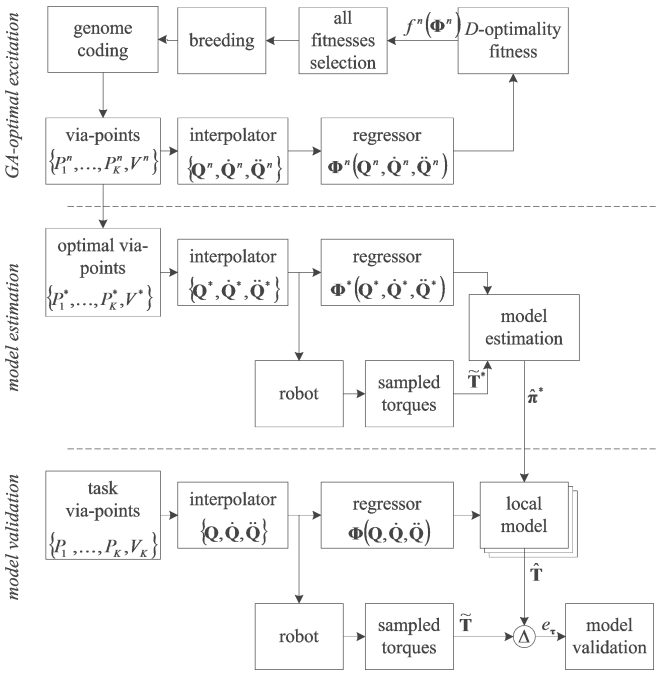

Fig. 2: The model estimation procedure (mid-layer) computes the parameters using an optimized excitatory, which is pre-computed in through GA (top-layer). The obtained model is then evaluated along random trajectories (bottom-layer).

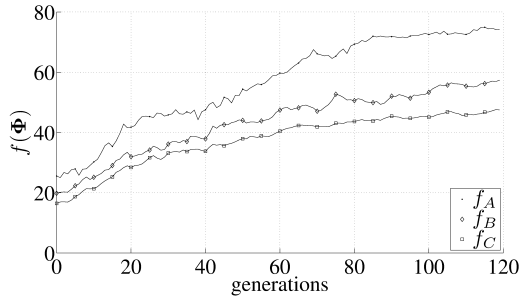

Fig. 3: Genetic Algorithm optimization results. Each fitness function f_A, f_B, f_C refers to the corresponding sub-regions of the workspace in Fig. 1.

B. Optimal Excitation Trajectory

The optimization problem formulation, *i.e.* identification of $\mathbf{\Phi}^\star = \mathbf{\Phi}(\mathbf{Q}^\star, \dot{\mathbf{Q}}^\star, \ddot{\mathbf{Q}}^\star)$, is derived from the requirements and constraints of industrial setups (see Fig. 1) :

1) finding a sub-optimal set of K via-points P^*;
2) finding the interpolation velocity V^* along which a trajectory is calculated by standard IR motion planner.

Hence, the optimization grounds on the definition of a workspace sub-region that bounds the K desired interpolated via-points. Hereafter, the optimization goal will be indicated as the set $\{P_1^\star, \ldots, P_K^\star, V^*\}$.

The optimal via-points and the interpolation velocity are obtained from a Genetic Algorithm (GA hereafter) search over sets of candidate individuals $\{P_1^n, \ldots, P_K^n, V^n\}$ (the superscript n indicates the individual index), whose interpolated trajectory and derived regressors $\mathbf{\Phi}^n$ are evolved over generations (see top layer in Fig. 2). The 6D coordinates of each of K via-points and the interpolation velocity are concatenated along a single individual genome of $(6\,K+1)$ genes ranging in $[0,1] \in \mathbb{R}$. Genotypes are linearly mapped into physical trajectory parameters according to particular ranges defined for each position/orientation coordinate and for minimum and maximum moving velocity. The population contains $N = 150$ genotypes (individuals), each carrying full information to code a trajectory. Generations following the first one are produced by a combination of selection with elitism, recombination and mutation [25]. The selection of individuals is made on a fitness function, commonly applied criteria are D-optimal or A-optimal fitnesses [13].

Drawback of such approaches relies on pure-kinematic nature of the regressor. In fact, generalized accelerations in $\mathbf{\Phi}$ could occasionally give comparable torques despite the relative exploitation of the maximum torque of different-sized actuators. Scaling the regressor with axis-wise ratios of nominal-over-maximum $\overline{\tau} = \max_i(\tau_{nom}^i)$ in order to normalize contributions of different actuators seems reasonable, and a torque-normalization of the regressor $\mathbf{H}(\mathbf{\Phi})$ whould remove dynamical biases due to the different motor contribution. Hence, denoting as $\mathbf{d} = diag(\tau_{nom}^1/\overline{\tau}, \ldots, \tau_{nom}^6/\overline{\tau})$, the observation matrix scaled results:

$$\mathbf{H}\left(\mathbf{\Phi}\right) = diag\left(\mathbf{d}, \ldots, \mathbf{d}\right)\, \mathbf{\Phi}. \tag{6}$$

Finally, in this case D-optimal fitness was considered maximizing the determinant of a quadratic form associated with $\mathbf{H}(\mathbf{\Phi}^n)$ of each n-th individual trajectory, *i.e.*

$$f^n\left(\mathbf{\Phi}^n\right) = \log_{10} \| \det\left[\mathbf{H}^t\left(\mathbf{\Phi}^n\right)\mathbf{H}\left(\mathbf{\Phi}^n\right)\right] \|. \tag{7}$$

III. Validation and Results

Method implementation and experiments are shown using a COMAU NS16 manipulator (see Fig. 1), with the C4G controller and the virtualizer of its interpolator *ORL - Open Realistic Robot Library*. The method has been validated in three different sub-regions of the workspace as displayed in Fig. 1.

A. Identified Excitation Trajectory

The identification of the excitatory trajectory resulted similar for all the three different experiment in the three different sub-regions of workspace (see Fig. 3) . They are characterized by a plain evolutionary process where the first generations show a fast convergence of the population to a family of trajectories yielding well-conditioned regressors. Along the saturation phase of the evolution, the best individuals and the population steadily improve their properties, while retaining consistency. This should due to the selective power of a fitness function that includes the scaling of the the regressor on the basis of nominal axes torques, avoiding major disruptions in terms of homogeneity in the interpolated trajectory. The three experiments differ for the maximum fitness value, nevertheless the optimized trajectory attained an excellent value for the regressor determinant (good mathematical conditioning of $\mathbf{H}$).

TABLE I: COMAU-NS16 robot.

Joint	1	2	3	4	5	6
Gear ratio	1/182	1/159	1/162	1/73	1/79	1/50
Torque Nom	3 Nm	6 Nm	3 Nm	.7 Nm	.7 Nm	.7 Nm

B. Dynamic Parameters Estimation

For each of the three sub-regions of the workspace, the genome (*i.e.* $\{P_1^\star, \ldots, P_K^\star, V^*\}$) calculated from the GA, has been loaded into NS16 interpolator obtaining the excitation trajectory $\{\mathbf{Q}^\star, \dot{\mathbf{Q}}^\star, \ddot{\mathbf{Q}}^\star\}$. $\widetilde{\boldsymbol{\tau}}$, $\widetilde{\boldsymbol{q}}$ and $\widetilde{\dot{\boldsymbol{q}}}$ have been sampled directly in the robot controller with a rate f_s =500 Hz (then filtered with a 8^{th}-order Butterworth filter with f_c =30 Hz) while accelerations $\widetilde{\ddot{\boldsymbol{q}}}$ have been numerically derived. Table II reports the results of the inversion of the measured system in (3), as in [24], for the three different experiment in the sub-region A, B and C. Looking through the table, some parameters show differences for many orders of magnitude in the three sub-regions.

C. Model Validation

For each of the three different sub-regions of the workspace displayed in Fig. 1, the validation of the evolved trajectory and consequently estimated parameters $\hat{\boldsymbol{\pi}}^\star$ is performed by moving robot along 30 trajectories, each defined by 6 via-points and interpolation velocity randomly calculated within the workspace sub-region as criteria described in section I and shown in Fig. 1. Sampled torques measured during each single trajectory test $\widetilde{\mathbf{T}}$ are then compared to estimated torques $\hat{\mathbf{T}}$ figured out of the locally calibrated model $\hat{\boldsymbol{\pi}}^\star$ (see bottom layer in Fig. 2) obtained from the optimal trajectory. The RMSE between estimated and sampled torques corresponds to the best estimator for the noise distribution in (4) and to a metric of the repeatability of the estimation over random test trajectories. Due to the inherently different contribution of each robot axis to the generated torque, so to the estimation noise, and the consideration of scaling discussed for the selected fitness function, the RMSE is expressed as:

$$\hat{\sigma}_\nu^{i,j} = \|\widetilde{\mathbf{T}}^{i,j} - \Phi^{i,j}(\widetilde{\ddot{q}}, \widetilde{\dot{q}}, \widetilde{q})\hat{\boldsymbol{\pi}}^\star\|_2 \,/\, S \tag{8}$$

where S is the number of samples in each $i = 1, \ldots, 30$ trajectories and $j \in (1, \ldots, 6)$ is the axis number. Then $\hat{\sigma}_\nu^{i,j}$ has been normalized out of each corresponding motor nominal torque transformed from motor side to joint side (NS16 gearmotors data are reported in Table I):

$$\hat{\sigma}_{\nu|norm}^{i,j} = \hat{\sigma}_\nu^{i,j} \,/\, \tau_{nom}^i \tag{9}$$

as in Fig. 8. Prediction error calculated in (8) is used in Figs. 4, 5, 6 to compute the upper and lower bounds for the predicted $\hat{\mathbf{T}}$ from $\hat{\mathbf{T}}^\star$, displaying the curves calculated as:

$$\hat{\mathbf{T}}^{i,j} \pm \hat{\sigma}_\nu^{i,j}. \tag{10}$$

D. Discussion

Analysis at a glance of Figs. 4, 5, 6, and of Table II displays (i) the predictive power of the rigid-multi-body model is extremely high, and (ii) the predictive power of the model is preserved in all the three experiments despite the parameters are strongly different in the three cases. The difference in magnitude (and sign) of many dynamic parameters in the different sub-regions A, B, C demonstrates as the lumped-rigid model is a partial model for an IR.

The inaccuracies in the prediction of the torques are partially relevant only for the last three axes (see Fig. 8) even if it should mainly related the low value of nominal motor torques (the magnitude error for the last three axis is less than 5Nm, Fig. 7). The inaccuracies in torque prediction should arise from an uncorrect friction model or from an uncorrect excitation of the friction parameters, *e.g.* in Fig. 5d, there is a significant error when actuator invert the rotation direction. Different model of static friction should improve the methods accuracy, although higher-model order should make more complex the convergence of the GA, and non linear models are not easy to be integrated in the method.

Besides considerations on friction, Fig. 8 displays that similar results are attained in all the three different sub-regions of the workspace despite the great differences in the fitness values (see Fig. 3). It could means that once the determinat of the regressor get high-value (*i.e.* the system is well conditioned) further increases do not affect the solution. Consequently, a position point on the quality of the selected fitness should be raised, and a different fitness improving the selection of trajectories more exciting the friction properties of the system should guarantee better performance.

Anyhow, *pros* and *contras* of the approach seems to confirm that the use of a GA is effective, and such definition of the genome (*i.e.* of the exciting trajectory as a series of a limited number of via-points), allows a straightforward representation of the task through its major template features, *i.e.* pose to visit and task space constraints in task execution.

IV. Conclusions

A procedure for local dynamic calibration has been introduced. Robot dynamic parameters are identified inside of task-dependent workspace sub-region. Experimental results confirm high accuracy in estimation of torques at joints, moreover prediction errors display good repeatability in parameters identification. The procedure is also easy to perform, allowing to frequently reload the calibration, in order to compensate parameters variations due to external phenomena. Future works will compare the accuracy reached through a local dynamic calibration and calibration defined for the complete workspace.

Acknowledgments

This work has been partially funded by ROBOFOOT European project (FP7-2010-NMP-ICT-FoF). Experimental activities have been partially supported by Roberto Bozzi, and Joao Carlos Dalberto, laboratory technicians of CNR-ITIA.

TABLE II: Parameters recombination is based on [11]. Denote as m_i is the mass of link, $mc_{r_i} = m_i\, r^i_{i,c_i}$ is the first-order moment of link i, r^i_{i,c_i} is the position from the origin frame i to the mass center of link i, I_i is the inertia tensor of frame i, $I_{m,i}$ is the inertia of ith actuator, $f_{0,i}$, $f_{1,i}$, $f_{2,i}$ are the coefficients for static and viscous friction of ith link. Constant coefficients related to robot geometry, are expressed in numerical form, in order to simplify table description, highlighting only dynamic parameters terms.

Index	Dynamic Parameter	Value		
		Sub-workspace A	Sub-workspace B	Sub-workspace C
1	mc_{2y}	5.599	1.355	1.996
2	I_{2xy}	-7234.289	-79.214	-237.628
3	I_{2yz}	-8.791	-9.712	26.252
4	I_{3xy}	-438.170	15.741	21.617
5	I_{3yz}	-544.750	19.227	-3.556
6	I_{3m}	-125.395	16.563	7.874
7	mc_{4x}	14.745	-0.007	1.399
8	I_{4xy}	-15.566	-3.858	-0.350
9	I_{4xz}	-113.245	-2.497	-2.049
10	I_{4m}	1.791	1.934	1.068
11	mc_{5x}	4.832	0.026	-0.020
12	I_{5xy}	2.969	0.280	0.158
13	I_{5xz}	4.457	-3.543	-0.884
14	I_{5yz}	17.141	0.039	-0.128
15	I_{5m}	15.853	3.223	2.936
16	mc_{6x}	- 4.631	0.003	-0.149
17	mc_{6y}	0.510	0.000	-0.026
18	I_{6xy}	0.615	0.169	0.140
19	I_{6xz}	0.914	0.036	0.049
20	I_{6yz}	0.652	-0.019	0.013
21	I_{6zz}	-1.122	-0.172	-0.171
22	I_{6m}	1.628	1.685	1.735
23	$I_{1yy} + I_{1m} + 0.090\, m_2 + I_{2yy} + 0.580\, m_3 + I_{3zz} + 0.614\, m_4 + 0.614\, m_5 + 0.614\, m_6$	17000.087	-519.146	-106.332
24	$mc_{2x} + 0.700\, m_3 + 0.700\, m_4 + 0.700\, m_5 + 0.700\, m_6$	48.251	69.585	69.772
25	$I_{2xx} - I_{2yy} - 0.490\, m_3 - 0.490\, m_4 - 0.490\, m_5 - 0.490\, m_6$	5671.557	500.779	-12.764
26	$I_{2xz} + 0.700\, mc_{3y}$	-58.448	-10.330	-3.755
27	$I_{2zz} + I_{2m} + 0.490\, m_3 + 0.490\, m_4 + 0.490\, m_5 + 0.490\, m_6$	403.981	104.790	121.765
28	$mc_{3x} + 0.185\, m_4 + 0.185\, m_5 + 0.185\, m_6$	47.010	10.768	8.776
29	$mc_{3z} + mc_{4y} + 0.624\, m_5 + 0.624\, m_6$	-33.218	13.335	14.261
30	$I_{3xx} - I_{3zz} - 0.034\, m_4 + I_{4zz} + 0.355\, m_5 + 0.355\, m_6$	-18709.585	373.346	272.356
31	$I_{3xz} - 0.185\, mc_{4y} - 0.115\, m_5 - 0.115\, m_6$	15379.696	-4.285	90.878
32	$I_{3yy} + 0.034\, m_4 + I_{4zz} + 0.423\, m_5 + 0.423\, m_6$	231.925	7.668	22.682
33	$mc_{4z} - mc_{5y}$	3.207	-0.078	0.066
34	$I_{4xx} - I_{4zz} + I_{5zz}$	-76.050	-18.763	-44.040
35	$I_{4yy} + I_{5zz}$	-49.652	0.248	-0.124
36	$I_{4yz} + 0.624\, mc_{5y}$	-8.221	0.539	-0.234
37	$mc_{5z} + mc_{6z}$	19.046	0.458	1.369
38	$I_{5xx} - I_{5zz} + I_{6yy}$	46.813	9.082	2.923
39	$I_{5yy} + I_{6yy}$	-19.608	0.044	-0.399
40	$I_{6xx} - I_{6yy}$	-0.578	0.496	0.058
41	$f_{0,1}$	16.146	40.510	54.952
42	$f_{0,2}$	4.783	1.242	1.299
43	$f_{0,3}$	55.554	63.050	64.111
44	$f_{0,4}$	1.825	2.590	2.418
45	$f_{0,5}$	37.579	44.440	42.601
46	$f_{0,6}$	1.531	1.101	1.047
47	$f_{1,1}$	5.044	6.251	7.218
48	$f_{1,2}$	-0.043	0.104	0.054
49	$f_{1,3}$	8.861	8.376	10.104
50	$f_{1,4}$	0.509	0.284	0.261
51	$f_{1,5}$	3.488	6.633	7.292
52	$f_{1,6}$	-0.016	0.073	0.067
53	$f_{2,1}$	21.871	-9.946	1.694
54	$f_{2,2}$	-13.890	-17.852	-10.439
55	$f_{2,3}$	19.751	-14.765	-4.847
56	$f_{2,4}$	6.157	4.954	7.541
57	$f_{2,5}$	4.658	3.094	5.138
58	$f_{2,6}$	2.659	6.054	8.073

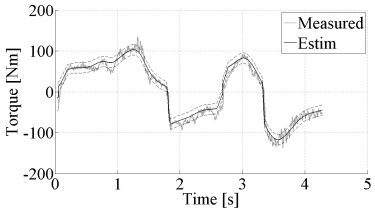

(a) *Axis 1*.

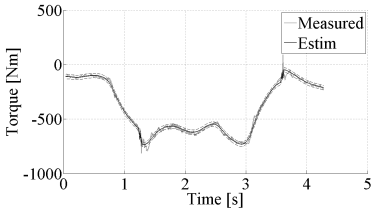

(b) *Axis 2*.

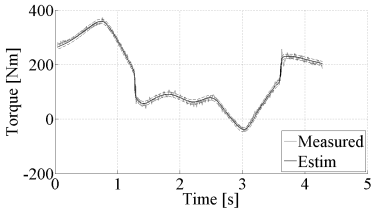

(c) *Axis 3*.

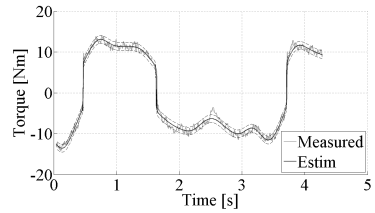

(d) *Axis 4*.

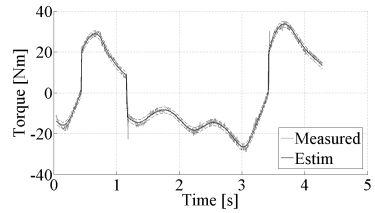

(e) *Axis 5*.

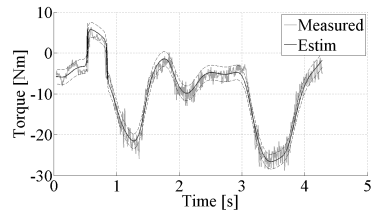

(f) *Axis 6*.

Fig. 4: Sub-workspace A (see Fig. 1). Measured torques $\widetilde{\mathbf{T}}$ in one of the 30 trajectories compared with the estimated one $\hat{\mathbf{T}}$. In addition bound curves calculated in (10) is displayed.

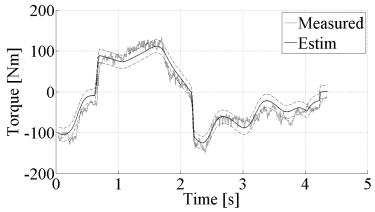

(a) *Axis 1*.

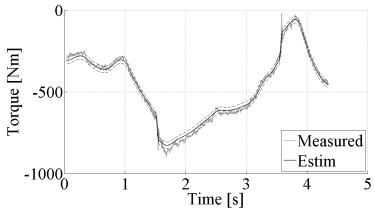

(b) *Axis 2*.

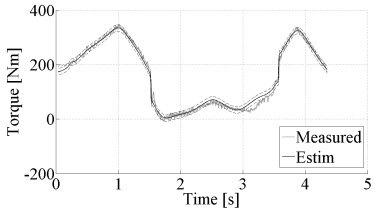

(c) *Axis 3*.

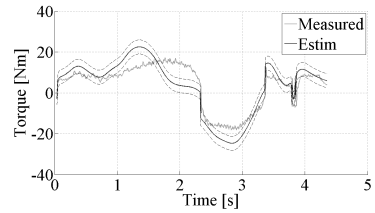

(d) *Axis 4*.

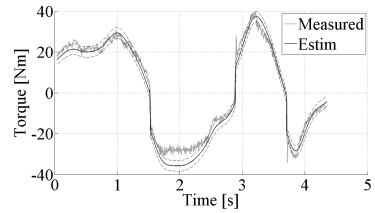

(e) *Axis 5*.

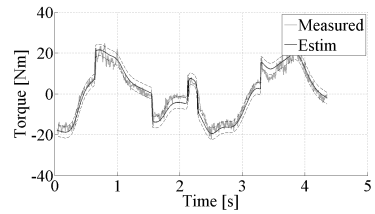

(f) *Axis 6*.

Fig. 5: Sub-workspace B (see Fig. 1). Measured torques $\widetilde{\mathbf{T}}$ in one of the 30 trajectories compared with the estimated one $\hat{\mathbf{T}}$. In addition bound curves calculated in (10) is displayed.

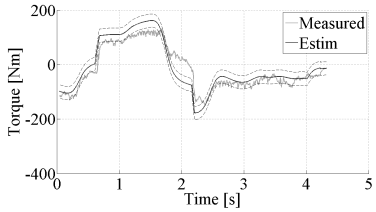

(a) *Axis 1*.

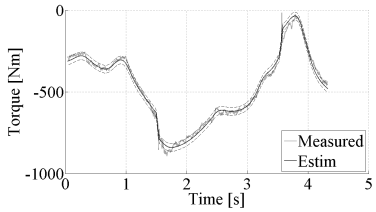

(b) *Axis 2*.

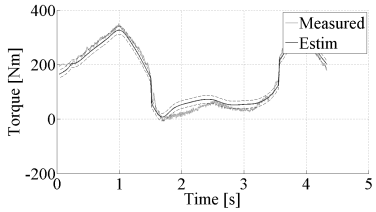

(c) *Axis 3*.

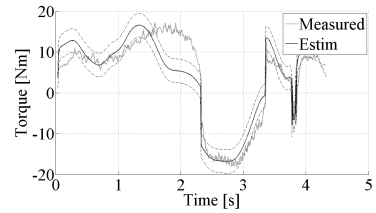

(d) *Axis 4*.

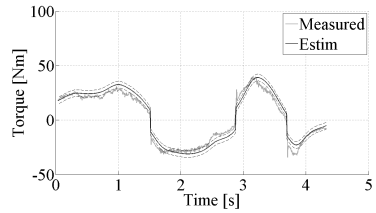

(e) *Axis 5*.

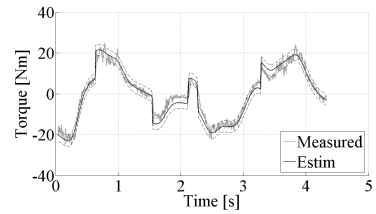

(f) *Axis 6*.

Fig. 6: Sub-workspace C (see Fig. 1). Measured torques $\widetilde{\mathbf{T}}$ in one of the 30 trajectories compared with the estimated one $\hat{\mathbf{T}}$. In addition bound curves calculated in (10) is displayed.

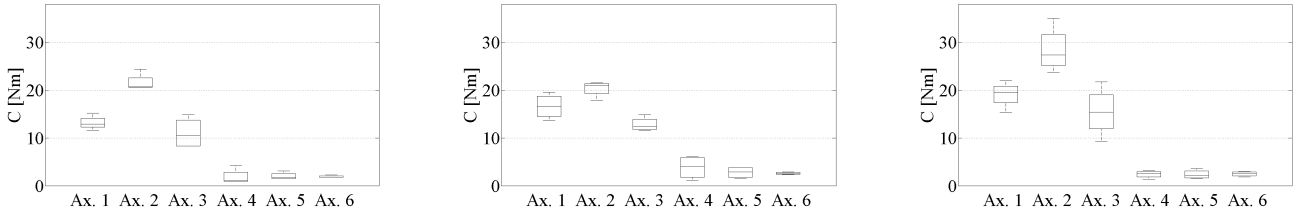

Fig. 7: Validation: 30 randomly generated trajectories. Distribution of prediction error $\hat{\sigma}_\nu$ for each motors as (8).

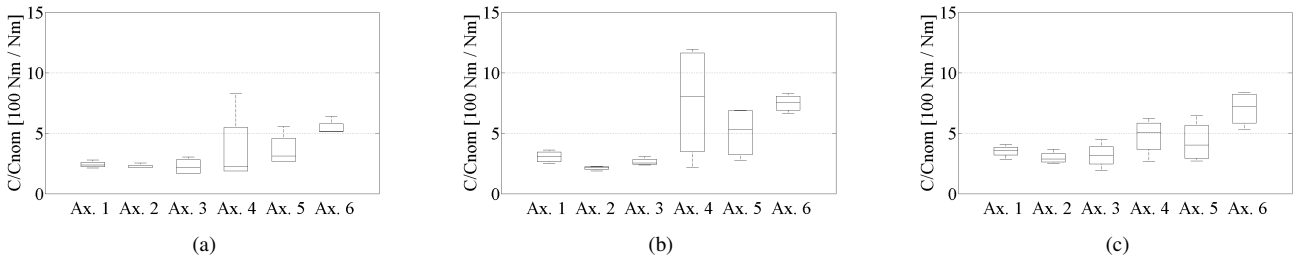

Fig. 8: Validation: 30 randomly generated trajectories. Distribution of normalized prediction error $\hat{\sigma}_\nu$ for each motors as (9).

REFERENCES

[1] P. K. Khosla and T. Kanade, "Experimental evaluation of nonlinear feedback and feedforward control schemes for manipulators," *The Int. J. of Robotics Research*, vol. 7, no. 1, pp. 18–28, 1988.

[2] P. Chiacchio, L. Sciavicco, and B. Siciliano, "The potential of model-based control algorithms for improving industrial robot tracking performance," in *Intelligent Motion Control, 1990. Proc. of the IEEE Int. Workshop on*, vol. 2, aug 1990, pp. 831 –836.

[3] F. Caccavale and P. Chiacchio, "Identification of dynamic parameters and feedforward control for a conventional industrial manipulator," *Control Engineering Practice*, vol. 2, no. 6, pp. 1039 – 1050, 1994.

[4] C. G. Atkeson, C. H. An, and J. M. Hollerbach, "Estimation of inertial parameters of manipulator loads and links," *The Int. J. of Robotics Research*, vol. 5, no. 3, pp. 101–119, 1986.

[5] M. Gautier and W. Khalil, "On the identification of the inertial parameters of robots," in *Decision and Control, 1988., Proc. of the 27th IEEE Conf. on*, vol. 3, dec 1988, pp. 2264 –2269.

[6] ——, "Exciting trajectories for the identification of base inertial parameters of robots," *The Int. J. of Robotics Research*, vol. 11, no. 4, pp. 362–375, 1992.

[7] J. Swevers, C. Ganseman, D. Tukel, J. de Schutter, and H. Van Brussel, "Optimal robot excitation and identification," *Robotics and Automation, IEEE Transactions on*, vol. 13, no. 5, pp. 730 –740, oct 1997.

[8] K.-J. Park, "Fourier-based optimal excitation trajectories for the dynamic identification of robots," *Robotica*, vol. 24, no. 5, pp. 625–633, 2006.

[9] B. Armstrong, "On finding exciting trajectories for identification experiments involving systems with nonlinear dynamics," *The Int. J. of Robotics Research*, vol. 8, no. 6, pp. 28–48, 1989.

[10] C. Presse and M. Gautier, "New criteria of exciting trajectories for robot identification," in *Rob. and Aut., Proc., IEEE Int. Conf. on*, may 1993, pp. 907 –912 vol.3.

[11] G. Antonelli, F. Caccavale, and P. Chiacchio, "A systematic procedure for the identification of dynamic parameters of robot manipulators," *Robotica*, vol. 17, no. 04, pp. 427–435, 1999.

[12] X. Hong, C. Harris, S. Chen, and P. Sharkey, "Robust nonlinear model identification methods using forward regression," *Systems, Man and Cybernetics, Part A: Systems and Humans, IEEE Transactions on*, vol. 33, no. 4, pp. 514 – 523, july 2003.

[13] G. Calafiore, M. Indri, and B. Bona, "Robot dynamic calibration: Optimal excitation trajectories and experimental parameter estimation," *J. of Robotic Systems*, vol. 18, no. 2, pp. 55–68, 2001.

[14] N. D. Vuong and M. H. J. Ang, "Dynamic model identification for industrial robots," *Acta Polytechnica Hungarica*, vol. 6, no. 5, pp. 51–68, 2009.

[15] D. Bristow, M. Tharayil, and A. Alleyne, "A survey of iterative learning control," *Control Systems, IEEE*, vol. 26, no. 3, pp. 96 – 114, june 2006.

[16] A. Visioli, G. Ziliani, and G. Legnani, "Iterative-learning hybrid force/velocity control for contour tracking," *Robotics, IEEE Transactions on*, vol. 26, no. 2, pp. 388 –393, april 2010.

[17] M. W. Spong, S. Hutchinson, and M. Vidyasagar, *Robot Modeling and Control*. Wiley, 2006.

[18] B. Raucent and J. C. Samin, "Minimal parametrization of robot dynamic models," *Mechanics of Structures and Machines*, vol. 22, no. 3, pp. 371–396, 1994.

[19] P. Fisette, B. Raucent, and J. C. Samin, "Minimal dynamic characterization of tree-like multibody systems," *Nonlinear Dynamics*, vol. 9, pp. 165–184, 1996, 10.1007/BF01833299.

[20] M. Indri, G. Calafiore, G. Legnani, F. Jatta, and A. Visioli, "Optimized dynamic calibration of a scara robot," in *IFAC '02. 2002 IFAC Internation Federation on Automatic Control*, 2002.

[21] M. Gautier and W. Khalil, "Direct calculation of minimum inertial parameters of serial robots," *Robotics and Automation, IEEE Transactions on*, vol. 6, no. 3, pp. 368–373, 1990.

[22] F. Benimeli, V. Mata, and F. Valero, "A comparison between direct and indirect dynamic parameter identification methods in industrial robots," *Robotica*, vol. 24, no. 5, pp. 579–590, Sept. 2006.

[23] J. Wu, J. Wang, and Z. You, "An overview of dynamic parameter identification of robots," *Robotics and Computer-Integrated Manufacturing*, vol. 26, no. 5, pp. 414 – 419, 2010.

[24] M. Gautier, "Dynamic identification of robots with power model," in *Rob. and Aut., Proc., IEEE Int. Conf. on*, vol. 3, 1997, pp. 1922 –1927.

[25] D. E. Goldberg, *Genetic Algorithms in Search, Optimization and Machine Learning*. Addison-Wesley, Reading, MA, 1989.